

Dendrites

Understanding of this familiar phenomenon has led to the development of useful man-made materials.

W. A. Tiller

The name *dendrite*, which comes from the Greek word for *tree*, has been given to a "tree-like" crystal morphology often observed in nature—in the patterns of snow flakes, of geological formations, and of ice as it develops on ponds. Recent technological research and the furnaces of industry have made many new contributions to the family of dendrites.

Dendritic growth is exhibited by a wide variety of materials (Figs. 1 and 2), and the form is natural to all of the dominant phase transformations—crystallization from the melt or from liquid or solid solutions, crystallization from the vapor, or electrocrystallization. The growth of understanding of such crystal forms helps us to recognize the place that the dendritic morphology of a material occupies among the possible morphologies that a crystal can develop and to understand under what environmental conditions this particular crystal morphology dominates. We also see how a slight change in environmental conditions may cause a growing crystal to change from the dendritic form to an entirely different morphology and how vastly different morphologies can be generated by only slight differences in some of the important parameters that control the process of crystal growth.

A classic experiment illustrating

changes in crystal morphology that are associated with slight changes in environmental conditions is Mason's experiment on ice crystals grown from the vapor (1). He suspended a thin nylon or glass fiber vertically in a water-vapor diffusion chamber and allowed the temperature in the chamber to vary continuously along the length of the fiber. At a certain water-vapor pressure in the chamber, ice crystals formed on the fiber, and the crystals at different positions on the fiber developed different morphologies. These different crystal shapes, and the range of temperatures at which they formed, are given in Table 1. The simultaneous growth of the many crystal forms on the same fiber brought into relief the sharpness of the boundaries between one morphology and another. For example, the transition between plates and needles at -3°C and that between hollow prisms and plates at -8°C occurred within temperature intervals of less than 1° .

To fully appreciate the range of dendritic forms or filamentary forms (forms without side branches) that can arise during crystal growth, we must consider both isothermal, or unconstrained, crystal growth, where crystals grow freely in a large bath of liquid of constant temperature which is below the melting temperature of the crystal, and crystal pulling, or constrained crystal growth, where crystals grow from a bath of liquid held at a temperature above the melting temperature of the crystal.

Unconstrained Crystal Growth

Let us first consider the unconstrained growth of a crystal from a supercooled alloy melt (2) (see Fig. 3). In Fig. 3 (right), $T_L(C_2)$ is the equilibrium freezing temperature of the bulk liquid (the liquidus temperature), and T_2 is the actual temperature of the liquid far from the growing crystal. Due to the presence of solute atoms in the melt, a partitioning of solute occurs at the moving interface, and, because of the slow diffusion of these atoms, the solute concentration changes at the interface from C_2 to C_1 (C_1 depends upon freezing velocity, particle shape, and other factors). This change lowers the liquidus temperature of the crystal surface to $T_L(C_1)$. Since the growing particle is curved, a pressure due to capillarity is imposed upon the solid, lowering the equilibrium temperature of the solid from $T_L(C_1)$ to $T_B(C_1)$, the amount of lowering depending upon the average curvature of the crystal. Further, since the particle is growing, a certain departure from the equilibrium temperature, δT , must exist at the interface, to drive the molecular transfer from liquid to solid, so the actual interface temperature T_i is below T_B . Finally, the particle must be evolving latent heat as it grows, and T_i must be enough above the bath temperature to allow dissipation of heat to the bath.

The foregoing paragraph describes the subdivision of the total amount of supercooling, ΔT , into its component parts, ΔT_s , ΔT_B , δT , and ΔT_H , in a crystal growth situation in which no electric fields are applied to the system. All four components are involved in every such growth problem; however, certain ones dominate in different materials. In the growth of crystals from a relatively pure metal melt, ΔT_H is approximately equal to ΔT , so this growth is largely controlled by heat flow. During the growth of an oxide crystal from a melt of steel, for example, ΔT_s is approximately equal to ΔT , so the growth is largely diffusion-controlled. Finally, during the growth of a polymer crys-

The author, who was formerly affiliated with the Research and Development Center of Westinghouse Electric Corporation, Pittsburgh, Pa., is now professor in the department of materials science, Stanford University, Stanford, Calif.

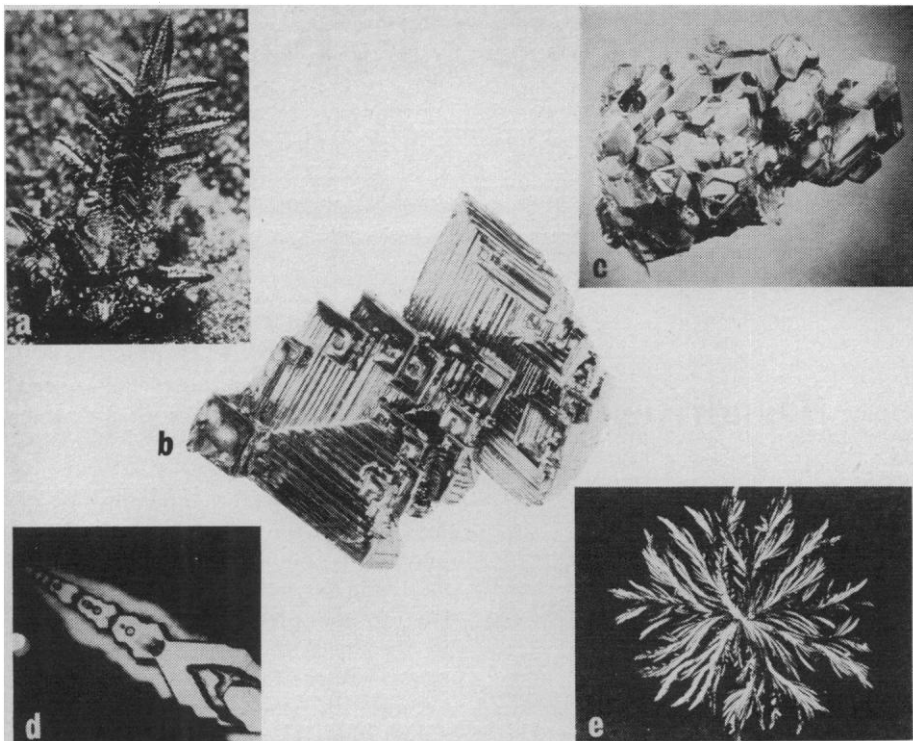


Fig. 1. Various crystal growth forms. (a) Chromium dendrite grown from the vapor; (b) bismuth hopper crystal grown from the melt (11); (c) gallium phosphide crystal grown from an alloy melt (12); (d) silver dendrite grown by electrodeposition (12); and (e) spherulite grown from a blend of 40 percent isotactic polypropylene and 60 percent atactic polypropylene (13).

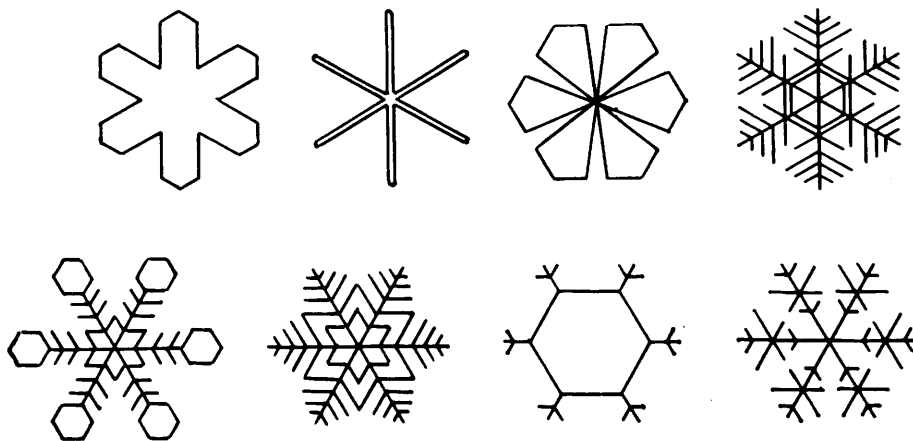


Fig. 2. Eight common snow crystal types.

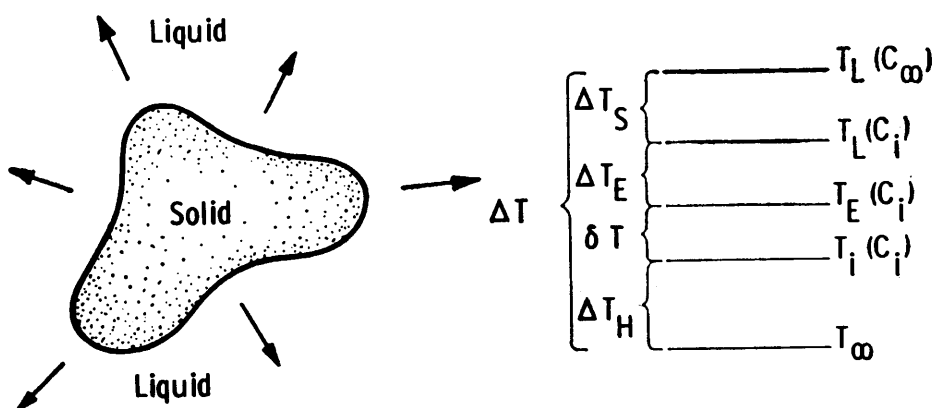


Fig. 3. (Left) A crystal growing from a supercooled liquid; (right) the important temperatures in the growth process. The magnitudes of the temperature differences indicate the degree of solute diffusion, capillarity, and kinetic or heat-transport control.

tal from a polymeric melt, δT is approximately equal to ΔT , and growth is largely controlled by the kinetics of interface attachment.

Now that we have considered the major factors that control the growth of any crystal from a melt, let us see what it is that determines which crystal morphology will dominate and, in particular, when the dendritic morphology will dominate.

An observer can test to find whether a particular crystal morphology is stable by applying perturbations of shape to the particle and observing whether the perturbations increase or decrease in amplitude with time. If they increase, the shape is unstable; if they decrease, it is stable. Let us consider the transition from a somewhat spherical particle shape to a spiked or predendrite shape, illustrated schematically in Fig. 4 and recorded for a polymeric system in Fig. 5. Growth of the amplitude of the perturbations relative to the main particle surface requires the creation of surface (increase in local curvature), so both ΔT_E and δT must increase in magnitude. Since ΔT is fixed, $\Delta T_S + \Delta T_H$ must decrease if the perturbations are to grow. It can be shown that the magnitudes of ΔT_S and ΔT_H are controlled by the same type of transport laws and that ΔT_S varies in the same fashion as ΔT_H in a particular case. Thus, a necessary condition for dendritic growth is that transport of heat or matter play an important role in the overall growth process and be more efficient for the dendritic shape than for other particle shapes. A sufficient condition for the existence of dendritic growth would be that the dendritic morphology allows crystal growth to proceed at a faster rate than any other crystal morphology does.

It may be quantitatively shown that a spherical particle undergoing transport-controlled growth into a supercooled bath will be unstable, when subjected to perturbations, when the radius of the sphere is greater than just 7 times the critical radius, R_c , predicted by homogeneous nucleation theory (3). It may be shown, further, that the rate of growth of a sphere of radius greater than about $100 R_c$ will be less than that of a well-developed dendrite-like particle having the shape of a paraboloid of revolution. The rate of growth for a particle of the latter shape depends much more upon the particular system under consideration than the rate for the sphere does. In general,

spheres of diameter greater than 10^{-3} to 10^{-2} centimeter develop the dendritic form.

Experimental evidence shows that dendrites generally grow with a constant axial velocity in certain specific crystallographic directions and develop side branches periodically at a particular distance back from the tip. These branches also grow axially in specific crystallographic directions. In order for freezing to occur at a constant axial rate $V(O)$, and for the dendrite to exhibit essentially constant form, the growth velocity normal to the surface at any point of the surface must be equal to the axial velocity $V(O)$ times the cosine of the angle ϕ between the two normals (see Fig. 6). Some distance back from the tip the dendrite begins to have approximately the shape of a cylinder, and, since ΔT_B and δT (Fig. 3, right) decrease here, by comparison with values for the tip, conditions develop which lead to the establishment of stable perturbations of shape in a lateral direction. These shape distortions eventually become side branches which, in turn, branch again when the appropriate conditions develop, and so on (4).

The thickness of the original dendrite stalk is largely determined by the con-

Table 1. Variation of ice crystal morphology with temperature.

Temperature ($^{\circ}\text{C}$)	Morphology
0°C to -3°C	Thin hexagonal plates
-3°C to -5°C	Needles
-5°C to -8°C	Hollow prisms
-8°C to -12°C	Hexagonal plates
-12°C to -16°C	Dendritic crystals
-16°C to -25°C	Plates
-25°C to -50°C	Hollow prisms

ditions prevailing at the tip, and, in many cases, the tip dimensions change freely and thus produce a change in the velocity of the dendrite. It has been shown quantitatively that bluntly tipped filaments freeze slowly and that sharply tipped filaments freeze rapidly. Given this freedom to change its tip dimensions, the most stable body shape should be that which has the maximum axial freezing velocity (4). From this postulate, the velocity V and the radius of curvature of the dendrite tips, ρ , as a function of bath supercooling ΔT , are given in Fig. 7 for ice, tin, nickel, and germanium dendrites. Because of the small radii of curvature, ρ , at the tip of the dendrites considered in Fig. 7, solute partitioning at the tip interface is very effective, and only a small solute buildup (k_o

< 1) or depletion ($k_o > 1$) occurs at the tip. Here, k_o is the phase-diagram partition coefficient of the solute. The solute distribution ahead of such an interface can be readily calculated for simple filament shapes like paraboloids of revolution or parabolic cylinders. In both these cases the surfaces are of constant concentration, and the ratio of C_l to C_s depends upon the shape, the dimensionless parameter $V\rho/D$ (D is the diffusion coefficient of the solute in the liquid), and the partition coefficient of the solute, k_o . In Fig. 8, $k/k_o (= C_l/C_s)$ is plotted against $V\rho/2D$ for a paraboloid of revolution with several values of k_o ; a parabolic cylinder would yield a value of C_l/C_s greater than the values given in Fig. 8 for the same value of $V\rho/2D$. The dendrite of maximum freezing velocity has a value for $V\rho/2D$ of approximately 1 to 2, so the solute concentration in the filament C_s , is generally much smaller than C_x for $k_o < 1$ and much greater than C_x for $k_o > 1$ ($C_s = kC_x$). Besides predicting the dendrite's dimensions, freezing velocity, and solute content as a function of the supercooling, one may also predict the crystallographic

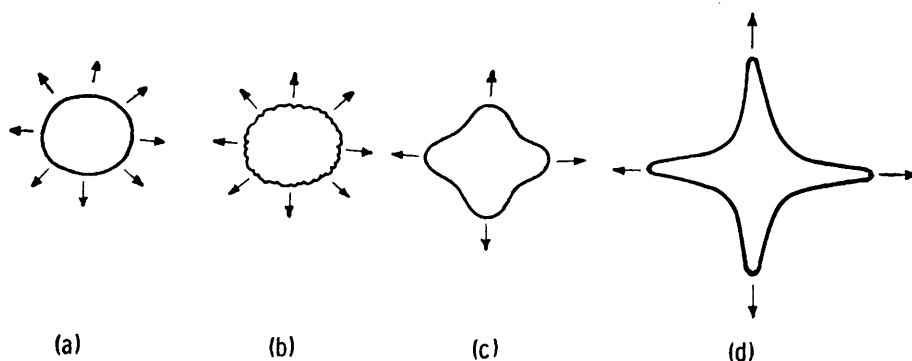


Fig. 4. The growth of shape perturbations on the sphere a as it transforms to the filamentary morphology d .

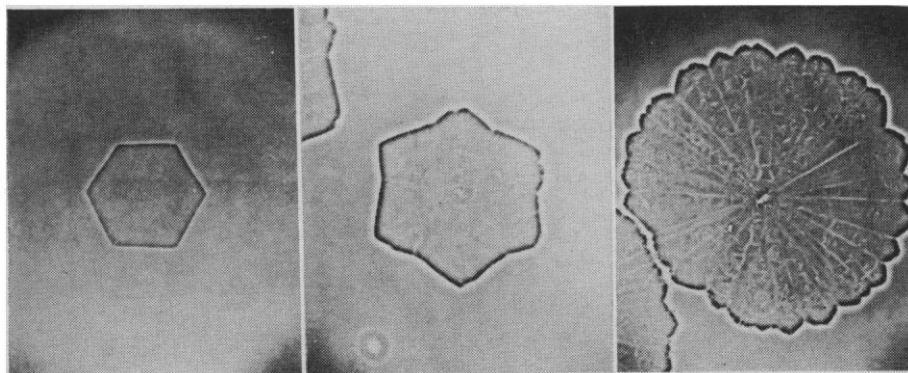


Fig. 5. Perturbation development on a hexagonal crystal of isotactic polystyrene (14).

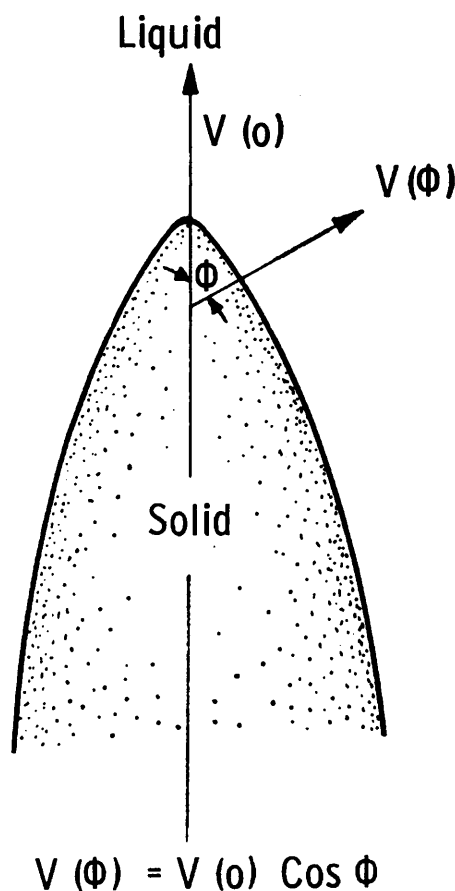


Fig. 6. Normal freezing-velocity variation with angle ϕ required for the "constancy of shape" condition.

orientation of the dendrites (that orientation which gives a maximum freezing velocity), provided one knows the molecular kinetics of interface attachment as a function of the crystallographic orientation. In general, we do not possess this information; however, by making certain reasonable assumptions concerning the kinetic anisotropy, we can deduce the directions of den-

drite growth for the metallic systems (4). In diamond-cubic materials—germanium and silicon, for example—one would expect the dendrite to be of square cross section and to grow most readily in the $\langle 100 \rangle$ direction. However, the molecular attachment kinetics are exceedingly slow on the $\{111\}$ faces comprising the tip of this

dendrite, and the growth of such a crystal form, as illustrated in Fig. 9a, is controlled by the attachment kinetics. In these materials, twin planes parallel to the $\{111\}$ planes form with low energy, so there is a finite probability that nucleation of such a twin will occur at the tip of the $\langle 100 \rangle$ dendrite. This would lead to the situation illustrated in Fig. 9b, where a reentrant

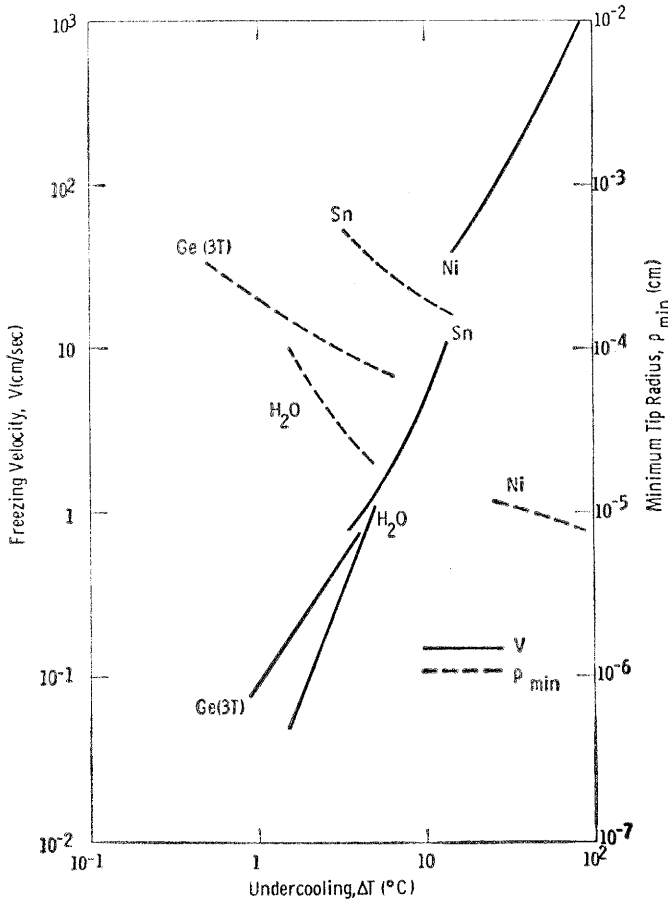


Fig. 7 (above). Plot of experimental data for freezing velocity of nickel, tin, water, and germanium (three-twin) dendrites and the radius of curvature at the tip, calculated from application of the maximum velocity condition.

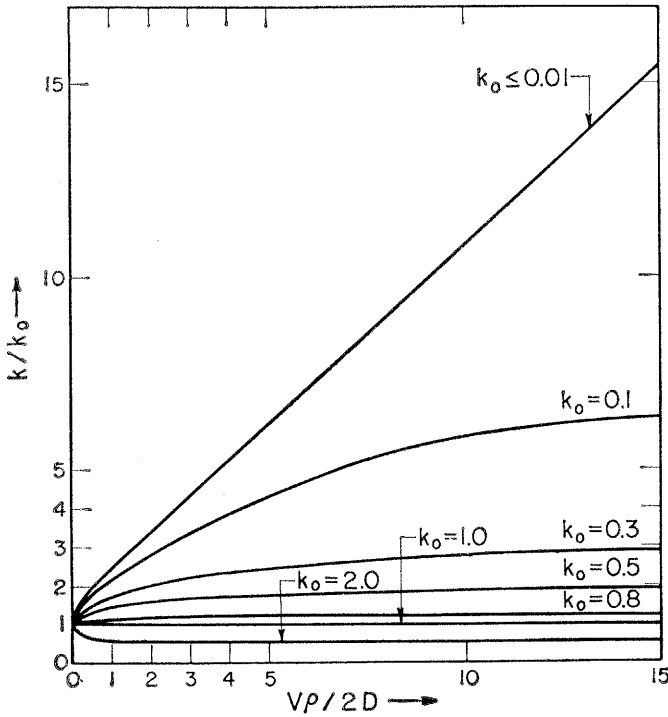


Fig. 8 (top right). Relative partition coefficient of the solute, $k/k_0 (=C_i/C_s)$, for a filament having the shape of a paraboloid of revolution, freezing at constant axial velocity V , as a function of $V\rho/2D$ for several values of k_0 (ρ is the radius of curvature of the tip of the filament).

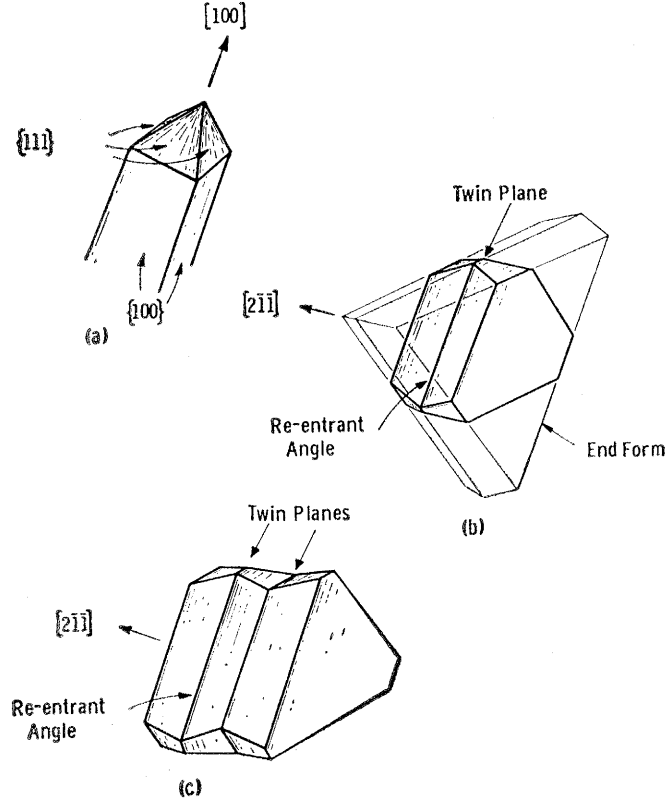


Fig. 9 (bottom right). Schematic drawing of some growth forms developed by diamond cubic materials as a function of their twin content: (a) no twins; (b) one twin; (c) two twins.

Fig. 10 (top right). Some twinned growth forms: (a) solution-grown, five-twinned, star-shaped, silicon growth form (5); (b) melt-grown germanium dendrite tip; (c) melt-grown germanium dendrite; (d) solution-grown indium arsenide (5); (e) vapor-grown twinned germanium plate (5); (f) melt-grown germanium dendrite body.

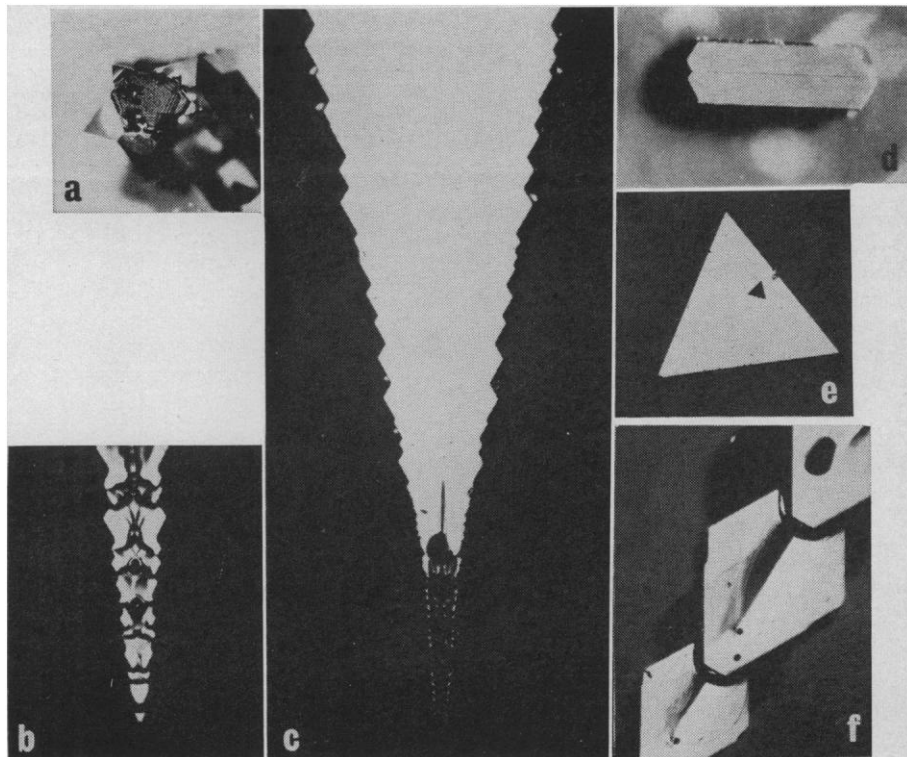
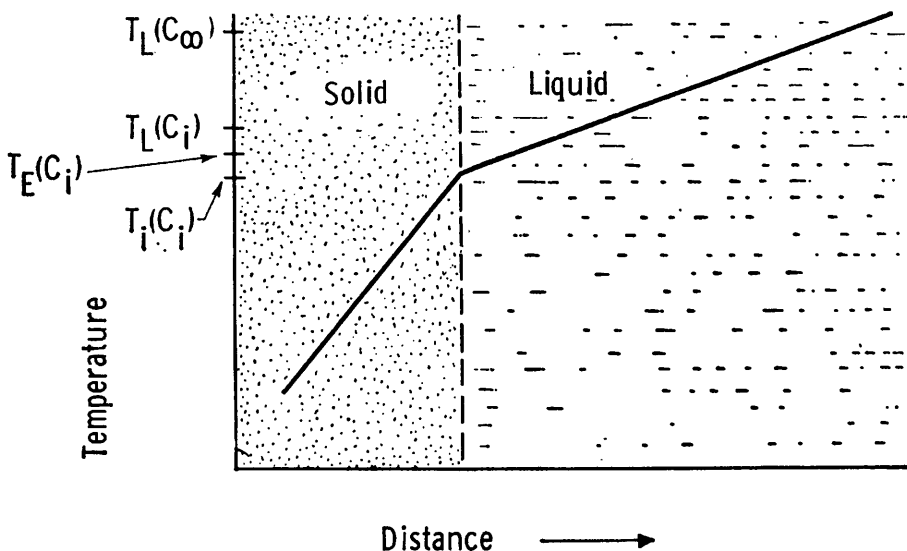


Fig. 11 (center right). Representation of the temperature distribution in the vicinity of the solid-liquid interface for the case of constrained crystal growth.

Fig. 12 (bottom right). Filament and dendrite formation during constrained crystal growth: (a) filament growth at an ice interface (potassium chromate solution); (b) photomicrograph of a decanted interface of a lead crystal solidifying from a melt of lead and a small amount of silver (5×10^{-4} weight percent); (c) ice bicrystal grown from very dilute hydrogen chloride solution, photographed with polarized light; (d) onset of side-branched development on ice filaments (2 atomic percent sodium chloride solution); (e) direct observation of dendrite formation in ice.



corner is created by the twin, allowing faster nucleation of crystal layers in this reentrancy. However, a single twin does not provide continuous propagation but, rather, leads to an end form, and it is only when two or more parallel twins form, as illustrated in Fig. 9c, that continuous propagation is possible. This multi-twinned filament (Fig. 9c) has a higher free energy per unit volume than the $\langle 100 \rangle$ filament; however, because the kinetics are more advantageous, this filament can propagate much faster than the $\langle 100 \rangle$ filament and is the one generally observed. In Fig. 1 a twinned silver dendrite grown by electrodeposition is shown. Figure 10 shows several twinned dendrites and other growth forms solidified from pure melts and alloy melts.

A great many crystal systems develop a twinned character when the molecular-attachment aspect of particle growth begins to dominate. For the growth of long dendritic ribbons, such as the ribbon of germanium in Fig. 10, it is necessary that a twin plane in the crystallographic system be parallel to a face of the equilibrium form. For systems exhibiting equilibrium forms completely closed by one set of facet planes, at least two parallel twin planes are required for continuous growth; for systems where stable equilibrium facets do not form a closed body, only one twin plane may be needed for continuous growth. In Table

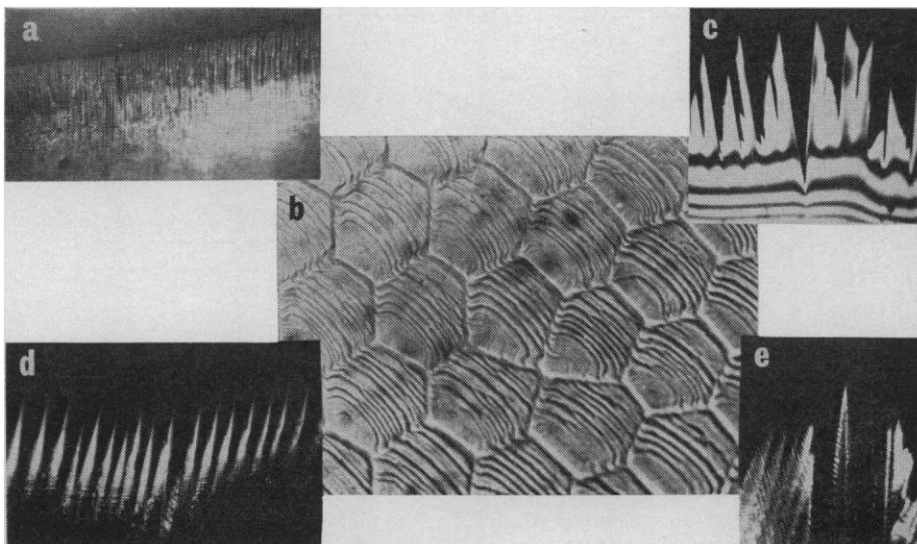


Table 2. Conditions for continuous dendrite growth.

Crystal structure	Equilibrium face	Twin plane	System	Minimum No. of twins
Diamond cubic and zinc blende	{110}	{111}	Closed	2
	{111}, {113}	{111}	Open	1
Face-centered cubic	{111}	{111}	Closed	2
Body-centered cubic	{101}	{112}	Closed	
Hexagonal close-packed	{0001}	{10 $\bar{1}$ 2}	Open	1
Hexagonal close-packed	{0001}	{0001}	Open	
Orthorhombic	{110}	{110}	Open	1
Rhombohedral	{110}	{110}	Open	1

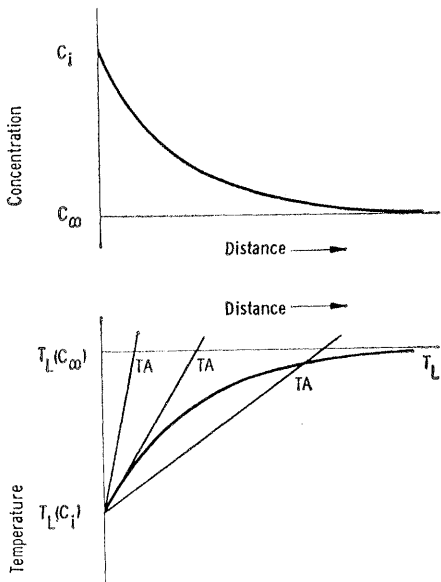


Fig. 13. (Top) Plot of the solute distribution in the liquid ahead of an advancing interface; (bottom) plot of the liquidus temperature T_L , and of several possible actual temperatures T_A , in the liquid ahead of the advancing interface.

2 is given the minimum number of twin planes needed for continuous or ribbon growth in various crystallographic systems (5).

Constrained Crystal Growth

Now let us consider dendrite formation and the dendrite morphology developed during constrained crystal growth. During constrained crystal growth from the melt the temperature in the liquid ahead of the solid-liquid interface increases with distance, and freezing is caused by producing the proper relative motion between a point in the solid and the freezing-point isotherm $T_L(C_i)$. The temperature distribution for this case is given in Fig. 11. Under certain freezing conditions the interface separating solid and liquid is macroscopically smooth, whereas under other conditions it exhibits the filamentary character seen in

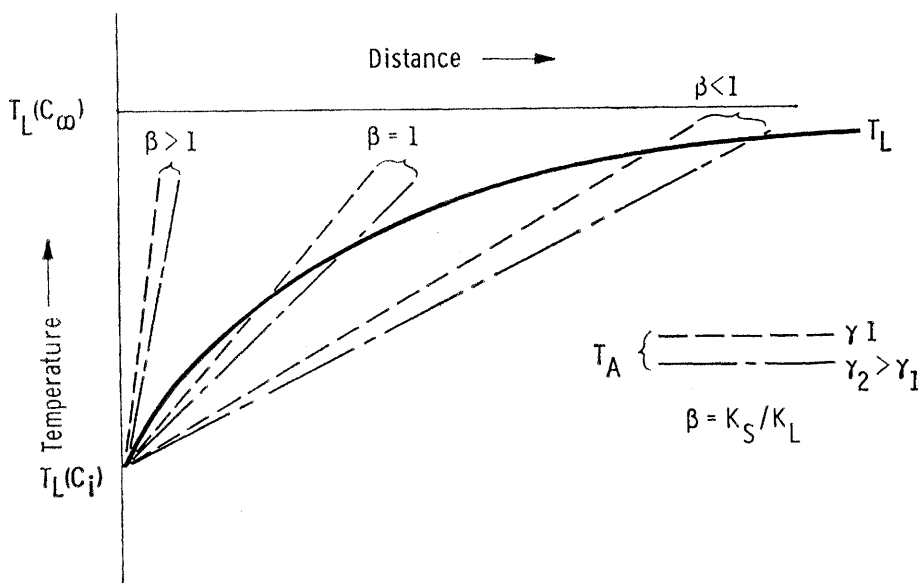


Fig. 14. Qualitative representation of sufficient conditions for stable filament growth in systems with interfacial energy $\gamma \neq 0$ and thermal conductivity ratio $\beta \neq 1$.

Fig. 12 (as determined by direct observation of ice freezing), or the cellular character detected indirectly by decanting the liquid from the solid during the freezing of a metal (2). In the latter method only a small part of the liquid is decanted from the interfilament space, hence the filament development is less clearly detected than in transparent media. This morphological transition has been detected in metal, semiconductor, oxide, and polymer crystals grown in this fashion, and it is associated with the development of an instability condition termed "constitutional supercooling."

Because of the partitioning of solute at the interface during freezing, the solute content of the liquid at the interface, C_i , is different from that in the bulk, C_∞ , and the liquidus temperature for the interface, $T_L(C_i)$, is lower than that for the bulk, $T_L(C_\infty)$. This is illustrated in Fig. 13. Superimposed upon the plot of $T_L(C)$ in Fig. 13 (bottom) are several possible actual temperature distributions, T_A ; here, ΔT_N and δT have been set at zero for simplicity. If T_L is greater than T_A , the liquid ahead of the interface is at a temperature below the liquidus temperature and is said to be constitutionally supercooled.

In order for shape perturbations to increase and transform the interface to a filamentary morphology, portions of the interface must be capable of moving ahead of the main interface. Since the curvature of such protrusions lowers the equilibrium temperature of the leading edges below that of a planar surface, the protrusions can only be stable if a sufficient lateral diffusion of solute occurs to raise the liquidus temperature by an amount greater than the incremental decrease due to curvature. Thus, a necessary condition for dendrite formation in this constrained-growth situation is that transport of solute play an important role in the overall growth process. A sufficient condition for the existence of a filamentary interface is that this morphology will allow the solid to intrude a greater distance into the liquid than any other interface morphology will.

It has been postulated that the onset of "constitutional supercooling" is a sufficient condition for filamentary interface formation. However, careful theoretical analyses have shown that this is only approximately true and that the transition from a smooth interface

to a filamentary interface depends upon the ratio of thermal conductivities of the solid and liquid, K_s and K_l , and the solid-liquid interfacial energy, γ (2, 6). Figure 14 shows qualitatively the sufficient conditions for stable increase in the perturbation amplitude for systems with $K_s/K_l > 1$, $K_s/K_l = 1$, and $K_s/K_l < 1$. If $K_s/K_l = 1$ and $\gamma = 0$, the instability is described by the onset of constitutional supercooling and is given quantitatively by

$$\frac{G}{V} \geq \frac{-mC_1(1-k_0)}{D} \quad (1)$$

where G is the temperature gradient in the liquid at the interface, V is the macroscopic freezing velocity, m is the phase-diagram liquidus slope, k_0 is the phase-diagram partition coefficient of the solute, and D is the diffusion coefficient of the solute in the liquid (2).

For the general range of values for K_s/K_l and γ that one observes, Eq. 1 is in error by a factor of about $\frac{1}{2}$ to 2. Equation 1 has been tested experimentally on several systems, and a plot of G/V against C_1 is indeed linear, deviating from the expected slope by no more than a factor of 2 (2). The transition from a smooth interface to a filamentary interface has been observed on gradually decreasing G and using the decanting technique. First, small protrusions form on the interface; next, irregular cell boundary grooves develop; then two-dimensional filaments are formed which change to a cellular array of filaments, and these eventually develop side branches as the degree of constitutional supercooling is increased.

In Eq. 1, C_1 is approximately equal to C_2/k_0 for the case of steady-state growth with a smooth interface, with

no fluid convection, and with k_0 small; it is possible to obtain this filamentary interface formation with C_2 approximately 0.1 to 1 part of solute per million parts of solvent. When such an interface forms, the filaments incorporate solute in a concentration C_s greater than k_0C_2 (slightly greater than that given by Fig. 8), and the average boundary concentration C_b is approximately $10 C_2(1-k_0)$. The maximum concentration at the boundary is usually the eutectic concentration, so it is not unreasonable to expect concentration ratios C_b/C_s of approximately 10^5 between the filament body and the interfilament space. Such high concentration ratios have a greater bearing on the electrical, optical, thermal, mechanical, and corrosion properties of the material.

"Colony formation" in a two-phase

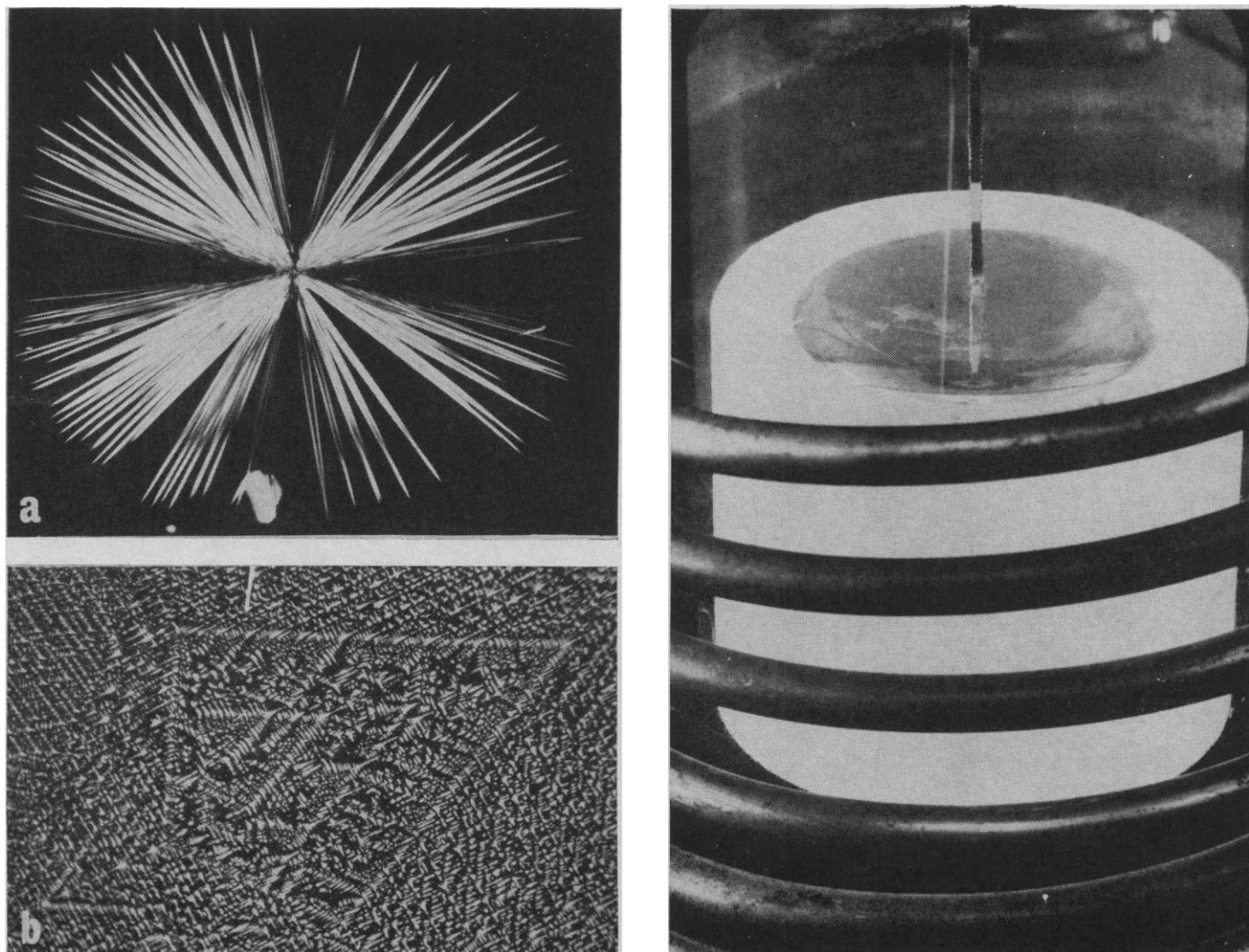


Fig. 15 (left). (a) Filamentary pattern of spherulite in malonamide containing 10 percent of *d*-tartaric acid (15); (b) photomicrograph of polished section for a lead-tin eutectic alloy solidified in a dendritic pattern. The white particles are tin, the black are lead (about $\times 78$). Fig. 16 (right). Photograph of the pulling of a germanium dendrite.

eutectic system and spherulite formation in polymeric systems are further examples of the constitutional supercooling instability resulting from the presence of alloying constituents. In Fig. 15, filament patterns for such systems are shown. For the broad range of materials studied, the filaments may be of circular, elliptical, or polyhedral cross section, depending upon the various anisotropies of the particular material under consideration. The arrays that the filaments generate are hexagonal, pentagonal, square, rectangular, or trigonal. Thus, the filament geometry seems to reflect the basic crystallography and the anisotropies of the crystal lattice, whereas, the array geometry seems to reflect some efficient packing criterion for such filaments.

Technological Applications

We might now ask, "How can this knowledge of dendritic growth be utilized to help build a greater materials technology than we have today?"

First, we can see that many desirable properties of a material will deteriorate if we allow a filamentary interface to form; thus, the environmental conditions that stabilize the filamentary interface morphology should be eliminated. This is true regardless of whether we are considering semiconductor or laser crystal formation, chemical crystallizers, or apparatus for converting saline water to pure water. Very recently industry has taken a more positive approach to this phenomenon and has considered how it might be utilized to produce materials of more desirable form than was hitherto possible. One great stride in this direction has been utilization of the technique of unconstrained crystal growth to produce long filaments of semiconductor crystals. A significant contribution to controlled dendritic growth was made by Bennett (7), who showed that a properly oriented, twinned seed crystal is necessary for well-controlled dendritic growth of germanium and silicon.

In the experimental set-up illustrated in Fig. 16 a graphite container filled with germanium is heated by means of an induction coil until the germanium melts; the power input is then controlled until the liquid is supercooled by an amount ΔT . If we allowed a seed crystal of dendritic orientation to be aligned perpendicular to the upper surface and then to be brought into con-

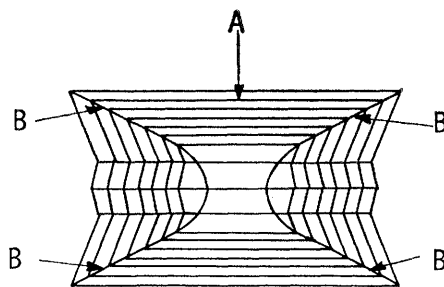


Fig. 17. Segregation traces in an idealized tip of a three-twin platelet.

tact with this surface, a dendrite would grow into this bath, colinearly with the seed crystal, at a velocity V . If the seed crystal were withdrawn from the bath at a velocity V , a long continuous filament of the material, of predictable thickness, could be pulled from the bath (8). Such a filament of germanium is being pulled from the melt in Fig. 16. For a bath supercooled by an amount $\Delta T = 10^\circ\text{C}$, filaments of metals, semiconductors, oxides, and polymers must be withdrawn at velocities, respectively, of approximately 10 cm/sec, 1 to 10^{-1} cm/sec, 10^{-1} to 10^{-2} cm/sec, and 10^{-2} to 10^{-4} cm/sec. The most convenient pulling velocity, in present practice, is about 10^{-1} to 1 cm/sec; the degree of supercooling of the bath, ΔT , must be

adjusted accordingly in order that stable filaments of the various materials may be pulled from the melt at velocities in this range.

Dendritic ribbons of germanium, silicon, and several of the III-V compounds have been pulled from the melt, and some of them have been wound on large reels to lengths of a hundred meters or so. These dendritic ribbons exhibit some chemical segregation in a rather intricate and consistent pattern, as illustrated in Fig. 17, and they can be so controlled as to yield relatively low dislocation densities. In Fig. 17 traces A and B represent an excess and a depletion, respectively, in solute concentration; such traces are not observed in undoped materials (9). The surfaces of the filaments appear to be perfect and to make ideal surfaces for fabrication of semiconductor devices. Electronic devices made upon such dendritic ribbons exhibit very satisfactory electrical characteristics.

Often during the pulling of semiconductor dendritic ribbons it was observed that two ribbons would grow side by side. At the lower pulling velocities a sheet of liquid was pulled from the melt and held between the dendrites by surface-tension forces. In the beginning, workers studying ribbon formation found this a nuisance; soon,

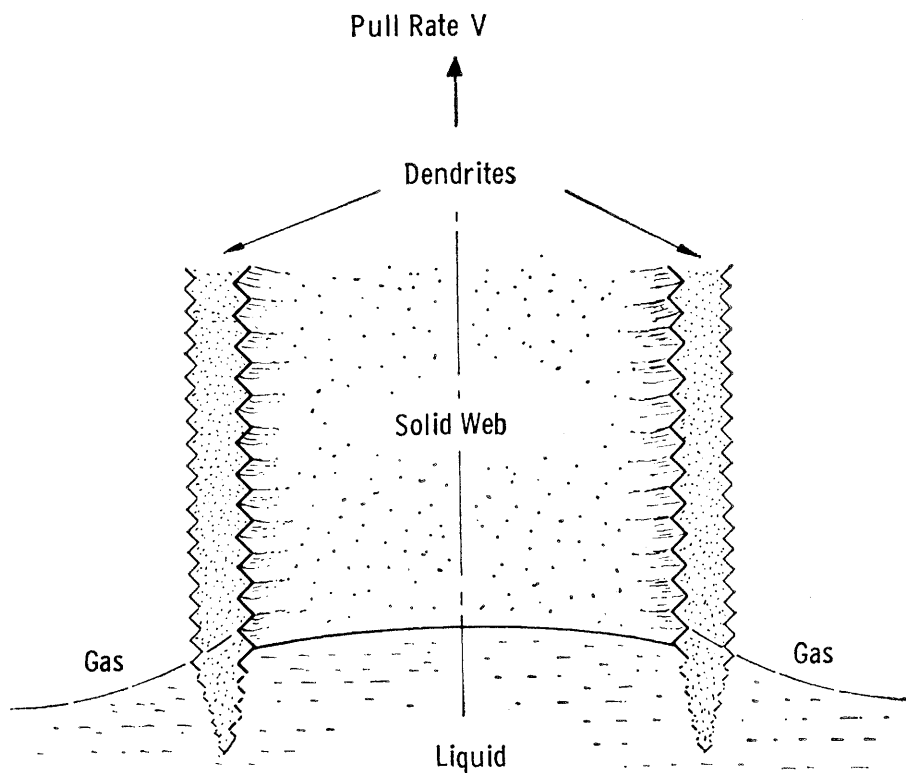


Fig. 18. Schematic representation of the dendrite and web configuration utilized in the continuous pulling of web material at velocity V .

however, some workers with an eye to possible applications recognized that the dendritic ribbons might be used as guiding edges for the formation of a sheet of semiconductor. It seemed possible that sheets of semiconductor of controlled thickness might be pulled, 1 to 2 centimeters wide rather than 0.1 centimeter, the width of the dendritic ribbons.

In Fig. 18 it may be seen that the dendrites at the edge grow below the surface of the supercooled melt and that the sheet grows above the normal surface of the melt. As the dendrites are pulled upward, molten material is drawn up by surface tension, the height of the freezing interface depending upon the furnace parameters (ΔT and the pull rate). The surface features and the internal structure of the sheets suggest that freezing at the interface takes place through a process similar to normal crystal growth. The dendrites at the edge, besides being necessary for growth of sheets of constant thickness, give stability to very thin sheets. Flat sheets can be pulled much thinner than dendrites; as the pull rate decreases, the thickness of the sheet increases, approaching the thickness of the dendrites. Sheets with more rounded surfaces can be grown even thicker than the dendrites (10).

After a period of developmental study, extremely long continuous sheets of germanium and silicon, up to 2 centimeters wide at thicknesses of 10 to 750 microns, were grown. A short length of such a web is shown in Fig. 19. This material was single-crystal in structure; the dislocation content was extremely low, and the surfaces were so perfect that they could be used without further treatment for fabrication of electronic devices. Diodes, transistors, and PNP devices have been fabricated on germanium and silicon, and large-area solar cells have been constructed on silicon. All such devices made on good webs and ribbons

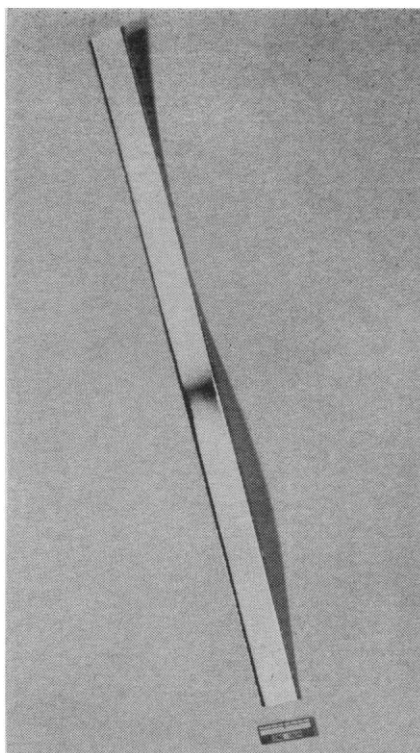


Fig. 19. Photograph of a short length of silicon ribbon about 2 centimeters wide.

were found to be as good as, or better than, the best devices made on conventional material. It thus seems that such processes possess considerable potential for the preparation of silicon and germanium and that efforts directed toward more complete utilization of the web-growing process, as opposed to the conventional crystal-growing process, are likely to be rewarding.

It is very likely that, in the future, more attention will be paid to the process of dendritic growth for the preparation of long sheets of a particular material. Undoubtedly we will also eventually be able to utilize dendrite formation in the constrained-growth situation to produce large crystals containing a polygonal array of filaments, all with the same physical characteristics, which are separated from, and

cemented to, each other by a matrix having a different set of physical characteristics.

Summary

I have touched upon the great variety of crystal forms and dendritic forms in nature, have discussed the essential physics involved in the generation of these forms during either constrained or unconstrained crystal growth, and have shown how this knowledge helps in the classification of this seemingly infinite variety of forms. Man has built upon this understanding to control the form and dimensions of certain materials to his technological advantage. We may hope that, in the future, we will have greater understanding of these phenomena of natural crystal growth and the ability to use this knowledge for technological ends.

References and Notes

1. B. J. Mason, in *Art and Science of Crystal Growing* (Wiley, New York, 1963), pp. 119-150.
2. W. A. Tiller, *ibid.*, pp. 276-312.
3. W. W. Mullins and R. F. Sekerka, *J. Appl. Phys.* **34**, 323 (1963).
4. G. F. Bolling and W. A. Tiller, *ibid.* **32**, 2587 (1961).
5. J. W. Faust, Jr., and H. F. John, *Trans. AIME*, in press.
6. W. W. Mullins and R. F. Sekerka, *J. Appl. Phys.* **35**, 444 (1964).
7. A. I. Bennett, British patent 889058; U.S. patent 3031403.
8. D. R. Hamilton and R. G. Seidensticker, *J. Appl. Phys.* **34**, 1450 (1963).
9. J. W. Faust, Jr., H. F. John, S. O'Hara, *Metallurgy of Semiconductor Materials*, J. B. Schroeder, Ed. (Interscience, New York, 1962).
10. S. O'Hara and A. I. Bennett, *J. Appl. Phys.* **35**, 686 (1964); S. N. Dermatis and J. W. Faust, Jr., *IEEE Trans. Commun. Electron.* **65**, 194 (1963).
11. R. S. Wagner and H. Brown, *Trans. AIME* **224**, 1185 (1962).
12. J. W. Faust, Jr., and H. F. John, private communication.
13. H. D. Keith and F. J. Padden, Jr., *J. Appl. Phys.* **35**, 1270 (1964).
14. ———, *ibid.* (June 1964).
15. ———, *ibid.* **34**, 2409 (1963).
16. I thank H. D. Keith, R. S. Wagner, J. W. Faust, Jr., and S. O'Hara for providing most of the photographs reproduced in this article, and, in particular, S. O'Hara for several helpful discussions. This work was partially supported by the Air Force Office of Scientific Research [contract AF 49(638)-1029].